Organic Electronics 13 (2012) 1329–1339

Contents lists available at SciVerse ScienceDirect

Organic Electronics

journal homepage: www.elsevier.com/locate/orgel

High-performance organic thin film transistors based on inkjet-printed polymer/TIPS pentacene blends

Song Yun Cho [a,*], Jung Min Ko [b], Jun-Young Jung [c], Jun Young Lee [b], Dong Hoon Choi [c], Changjin Lee [a,*]

[a] Advanced Materials Division, Korea Research Institute of Chemical Technology, 141 Gajeong-ro, Yuseong-gu, Daejeon 305-600, Republic of Korea
[b] Department of Chemical Engineering, Sungkyunkwan University, 300 Cheoncheon-dong, Jangan-gu, Suwon 440-746, Republic of Korea
[c] Department of Chemistry, Korea University, 145 Anam-ro, Seongbuk-gu, Seoul 136-701, Republic of Korea

ARTICLE INFO

Article history:
Received 7 December 2011
Received in revised form 8 March 2012
Accepted 1 April 2012
Available online 17 April 2012

Keywords:
Organic thin film transistor
Inkjet printing
TIPS pentacene
Triarylamine-based polymer
Polymer/TIPS pentacene phase separation
Flory–Huggins parameter

ABSTRACT

The blending of crystalline organic semiconductor, 6,13-bis(triisopropylsilylethynyl)-pentacene (TIPS pentacene) with amorphous polymers exhibits not only excellent solution processibility but also superior performance characteristics in organic thin film transistors (OTFTs). To understand the inkjet printing behavior of polymer/TIPS pentacene blends, we synthesized triarylamine-based polymers with various polarities, which were obtained by changing the fluorine content in the polymer structure. The variation of segregation strength of the polymer domains in the blends can be induced depending on the different polarities of the polymers, which can ultimately determine the shape and orientation of the TIPS pentacene crystals in OTFT films. This relationship was explained by the Flory–Huggins phase separation theory according to the measured TFT performance. Polarized optical microscopy, 3D surface profile, and X-ray diffraction (XRD) were used to investigate the crystal orientation, surface morphology, and crystallinity of the polymer/TIPS pentacene thin films. The experimental results suggest that the phase separation behavior between the polymer and TIPS pentacene plays a significant role in the formation of crystal structure of TIPS pentacene in the film. The moderate segregation of the polymers from the TIPS pentacene crystal domains effectively derives the desirable stripe-shaped crystals with the proper orientation and enhanced surface morphology. The resultant inkjet-printed films from the triarlyamine-based polymers with TIPS pentacene showed excellent mobility of 0.14–0.19 $cm^2 V^{-1} s^{-1}$, which are among the highest values obtained by inkjet printing reported to date.

© 2012 Elsevier B.V. All rights reserved.

1. Introduction

Solution-processed organic electronic devices have been attracting much attention because of their low-temperature and solution-based fabrication process without any vacuum steps, which therefore have the potential for low-cost, high-throughput fabrication over large areas on flexible substrates [1–5]. In particular, the field of printed electronics with inkjet printing is rapidly growing due to its additive, low-waste nature. Recently, TIPS pentacene has been the subject of intensive investigation for p-type OTFT active layer because of its low-cost solution processibility with high performance [6,7]. However, the localized high crystalline order of TIPS pentacene films leads to variations in hole mobility values across a single substrate. Many studies on inkjet printing TIPS pentacene have shown great deviation of mobility values over three orders of magnitude, which is mostly ascribed to the difficulty in controlling crystal growth when deposited from inkjet nozzles [8,9]. In order to solve this problem, TIPS pentacene blended with polymers has been used to reduce localized crystal anisotropy and to improve film uniformity. For example, OTFTs

* Corresponding authors. Tel.: +82 42 8607260 (S.Y. Cho), +82 42 8607208 (C. Lee).
E-mail addresses: scho@krict.re.kr (S.Y. Cho), cjlee@krict.re.kr (C. Lee).

1566-1199/$ - see front matter © 2012 Elsevier B.V. All rights reserved.
http://dx.doi.org/10.1016/j.orgel.2012.04.007

prepared from TIPS pentacene blended with poly(α-methylstyrene) have exhibited mobilities of about 0.1 $cm^2 V^{-1} s^{-1}$ and improved uniformity and thermal stability without degradation of electrical characteristics [10,11]. Furthermore, studies involving amorphous p-type polymer, poly(triarylamine) (PTAA) blended with TIPS pentacene have shown the good film-forming characteristics of PTAA and the high mobility of TIPS pentacene in OTFT devices [12,13].

However, the precise dependence of phase separation and performance of organic TFTs on the type and molecular structure of the polymers used has still not been clearly elucidated specifically for inkjet printing. Moreover, systematic and detailed studies on *inkjet-printed* TIPS pentacene-based TFTs have not been carried out. In this paper, we describe our initial attempt at inkjet printing the polymer/TIPS pentacene system to investigate the effect of the polymer structure on the phase separation of the polymer/TIPS pentacene and subsequent TFT performance. TIPS pentacene crystallization behavior in blends of polymer and TIPS pentacene is closely related to the phase separation between the polymers and TIPS pentacene, which suggests that the modification of the polymer structure that can affect the interaction between two components may have significant impact on the consequent inkjet printed OTFTs. Therefore, the microstructure of the polymer/TIPS pentacene film which results from the phase separation and TIPS pentacene crystallization is the key factor in determining the performance of TIPS pentacene-based OTFTs.

To investigate the dependence of field-effect mobility on various polymer structures, triarylamine-based homopolymers and copolymers with various ratios of pentafluorostyrene units were synthesized. The variation in the segregation strength between the polymer and TIPS pentacene phase can be dependent on the polarity difference between two components in the polymer/TIPS pentacene blend which can be easily manipulated by the number of C–F bonds in the polymer. We also believe that the crystallization process and sequent crystal orientation of TIPS pentacene in this system should be influenced by the segregation strength or the degree of phase separation between the polymer and TIPS pentacene. Even though it is difficult to analyze these segregation phenomena quantitatively, these different phase separation behaviors in relation to each polymer structure can be explained by applying the Flory–Huggins theory.

Triarylamine moieties were incorporated into the polymer side groups because it is well known that the existence of hole transporting triarylamine groups in PTAA can provide improved conduction pathways by enhanced hole injection in the active layer with the PTAA/TIPS pentacene-blended system [13]. Furthermore, bulky side groups, such as triarylamine groups dangling on the polymer chains, can assist the facile formation of more amorphous states of polymers, which can facilitate amorphous polymer/crystalline TIPS pentacene phase separation.

The crystal structure and thin film morphology of polymer/TIPS pentacene blends were observed by polarized optical microscopy, 3D profile, and XRD. Top-contact OTFTs were fabricated by the inkjet printing of the polymer/TIPS pentacene blends to determine device performance. Surprisingly, our polymer/TIPS pentacene systems showed considerably improved average mobility and stable performance of the inkjet-printed TIPS pentacene OTFTs. To the best of our knowledge, there have been no reports on the use of polymer/TIPS pentacene systems with such excellent TFT properties obtained by inkjet printing.

2. Experimental

2.1. Materials

4-Bromobenzene, tri-*tert*-butylphosphine, tris(dibenzylideneacetone) dipalladium(0), postassium *tert*-butoxide, and poly(pentafluorostyrene) were purchased from Aldrich and were used without any further purification. 4-Aminostyrene (TCI) and 2,3,4,5,6-pentafluorostyrene (Aldrich) were used after they were passed through a neutral alumina column to remove an inhibitor (*p-tert*-butylcatechol). TIPS pentacene was synthesized according to the procedure reported in an earlier publication [6]. Other solvents such as THF and toluene were purified by procedures described in the literature [14].

2.2. Instruments

^{1}H NMR measurements were conducted on a Brüker 300 MHz spectrometer. Thermogravimetric analyses were carried out with a Universal V4.5A TA Instruments TGA Q500 using 3–10 mg of samples. The temperature was raised from 30 °C to 700 °C at a heating rate of 10 °C/min in a nitrogen atmosphere with a gas flow rate of 50 mL/min. The thermal heat flow was monitored with a Universal V4.0C TA Instruments 2910 MDSC at a scan rate of 10 °C/min in nitrogen. The molecular weight distribution data were estimated using a Waters Alliance 2690 gel permeation chromatograph using PSS columns in THF as an eluent at a flow rate of 0.1 mL/min at 40 °C. The polar components of the polymers were determined using the contact angle measurements (SEO 300A, SEO Co., Korea) of the polymer films. Inkjet printing was carried out using a UNI-2100 inkjet printer (Unijet Co., Korea) under ambient room temperature conditions. Crystal images of TIPS pentacene of the inkjet-printed polymer/TIPS pentacene films were obtained with a Nikon Eclipse LV100 polarized optical microscope. To explore the fine surface roughness of the polymer/TIPS pentacene droplets and thin films, a 3D surface profiler (SIS-1200PLUS, SNU Precision Co., Korea) was employed in an area of 130 × 175 μm^2 using the non-contact mode. The average thickness of the inkjet-printed polymer/TIPS pentacene films was measured by α-step 500 (KLA Tencor Co., USA). To identify the crystal structures of TIPS pentacene, the polymer/TIPS pentacene films were analyzed via XRD (D/MAX-2200V, RIGAKU Co., Japan).

2.3. Synthesis of polymers

2.3.1. 4-Diphenylaminostyrene (1)

To a 250 mL vessel charged with tris(dibenzylideneacetone)dipalladium(0) (0.26 g, 0.44 mmol) and potassium

tert-butoxide (5.95 g, 53.04 mmol), 4-bromobenzene (8.33 g, 53.01 mmol), 4-aminostyrene (1.50 g, 12.59 mmol), tri-*tert*-butylphosphine (5.95 g, 53.04 mmol), and anhydrous toluene (180 mL) were successively added. The mixture was heated at 80 °C for 48 h with stirring under nitrogen ambient. When the flask reached room temperature, the solvent was evaporated on a rotary evaporator. The resulting solid was extracted with dichloromethane two times and dried over anhydrous $MgSO_4$. The crude products were purified by silica gel column chromatography eluted with hexane–ethyl acetate (100:1) to afford 2.25 g (66%) of **1** as a white powder. ^{1}H NMR ($CDCl_3$): δ 5.15 (d, 1H), 5.63 (d, 1H), 6.66 (dd, 1H), 7.01–7.30 (m, 14H).

2.3.2. Poly(4-diphenylamino)styrene (PDAS)

In a glove box, monomer **1** (0.45 g, 1.66 mmol), and free radical initiator 2,2′-azobisisobutyronitrile (AIBN) (0.0014 g, 0.0083 mmol) were dissolved in anhydrous THF (5 mL) in a pressure tube equipped with a magnetic stirring bar. The sealed tube was heated at 80 °C for 72 h under pressure. After the reaction was complete, the solvent was rotary-evaporated. The resulting solid was dissolved into a small amount of dichloromethane and precipitated into methanol and hexane twice to remove unreacted monomers and oligomers. After filtration, the polymer was isolated as a white powder (0.30 g, 66%). ^{1}H NMR ($CDCl_3$): δ 1.20–2.20 (br m), 6.10–7.20 (br m). M_n = 6 000, M_w/M_n = 2.3. T_g = 152 °C.

2.3.3. Poly[(4-diphenylamino)styrene-co-poly(pentafluorostyrene)] (PDA-PF 1)

In a glove box, monomer **1** (0.50 g, 1.84 mmol), 2,3,4,5,6-pentafluorostyrene (0.179 g, 0.922 mmol), and AIBN (0.002 g, 0.14 mmol) were dissolved in anhydrous THF (5 mL) in a pressure tube equipped with a magnetic stirring bar. The sealed tube was heated at 80 °C for 72 h under pressure. After the reaction was complete, the solvent was rotary-evaporated. The resulting solid was dissolved into a small amount of dichloromethane and precipitated into methanol and hexane twice to remove unreacted monomers and oligomers. After filtration, the polymer was isolated as a white powder (0.38 g, 55%). ^{1}H NMR (CD_2Cl_2): δ 1.60–2.90 (br m), 6.30–7.40 (br m). M_n = 17 000, M_w/M_n = 2.0. T_g = 146 °C.

2.3.4. Poly[(4-diphenylamino)styrene-co-poly(pentafluorostyrene)] (PDA-PF 2)

PDA-PF 2 was prepared via the same synthetic method as was used to prepare **PDA-PF 1**. The amounts of 2,3,4,5,6-pentafluorostyrene and AIBN used were 0.36 g (1.84 mmol) and 0.003 g (0.018 mmol), respectively. The polymer was isolated as a white powder (0.38 g, 44%). ^{1}H NMR (CD_2Cl_2): δ 1.60–2.90 (br m), 6.20–7.30 (br m). M_n = 17 000, M_w/M_n = 1.8. T_g = 137 °C.

2.3.5. Poly[(4-diphenylamino)styrene-co-poly(pentafluorostyrene)] (PDA-PF 3)

PDA-PF 3 was prepared via the same synthetic method as was used to prepare **PDA-PF 1**. The amounts of 2,3,4,5,6-pentafluorostyrene and AIBN used were 0.72 g (3.69 mmol) and 0.005 g (0.028 mmol), respectively. The polymer was isolated as a white powder (0.64 g, 53%). ^{1}H NMR (CD_2Cl_2): δ 1.60–2.90 (br m), 6.30–7.30 (br m). M_n = 20 000, M_w/M_n = 2.0. T_g = 141 °C.

2.4. Device fabrication

The fabricated OTFTs had bottom-gate top-contact architecture. The patterned indium tin oxide (ITO) substrates were used as gate electrodes. Those were cleaned by ultrasonification with a detergent solution (TICKOPUR R 33, DR. H. STAMM GmbH) and sequentially rinsed with deionized water, acetone, and isopropanol. Before the deposition of organic gate insulators, the substrates were treated with a UV-ozone plasma for 20 min. To prepare the solution of the photocurable organic gate insulator, 2,4,6-triallyloxy-1,3,5-triazine, pentaerythritol tetrakis(3-mercaptopropionate) (Aldrich) and Irgacure 369 (BASF) were mixed in propylene glycol monomethyl ether acetate (Aldrich). This solution was then spin-coated at 3000 rpm for 30 s and then UV (the intensity is >20 mW cm^{-2} at 254 nm) cured for 3 min. The deposited organic insulators had a specific capacitance of 94 pF/mm^2 at 1 kHz and a thickness of 440 nm. The capacitance of the dielectric layer was measured using a metal–insulator–metal (MIM, M = Au) structure [15] on an Agilent 4294A impedance analyzer. The active channel layer was deposited by inkjet printing the solution of TIPS pentacene blended with polymers of 1/1 by weight ratio at 1 wt.% concentration of solids in anhydrous toluene. The inkjet printer was controlled by 200 Hz (head frequency), 1000 DPI (resolution) and the nozzle diameter was set up for 30 μm. Inkjet printing was performed twice at 25 °C. After solvent drying in air, the deposited layer was annealed at 80 °C for 1 h on a hot plate in a glove box filled with nitrogen. The top-contact source and drain electrodes (75 nm thickness, Au) were thermally evaporated at 10^{-7} torr using a deposition rate of 1–2 Å/s through a patterned metal shadow mask. The ratio of the channel width and channel length was 20 (width: 1 000 μm, length: 50 μm). Electrical measurements were carried out in air using an Agilent 4155C semiconductor parameter analyzer. The field-effect mobility was calculated in the saturation region as,

$$\mu_{sat} = \frac{L}{W}\frac{1}{C_i}\frac{\partial^2 I_D}{\partial V_G^2} \quad (1)$$

where μ_{sat} is the saturation mobility, C_i (measured specific capacitance of organic gate insulator) is the geometric capacitance of the dielectric, and L and W are the channel length and width, respectively.

3. Results and discussion

A vinyl polymer with pendant moieties of triarylamine, poly(4-diphenylamino)styrene (**PDAS**) and their copolymers with pentafluorostyrene, poly[(4-diphenylamino)styrene-*co*-pentafluorostyrene]s (**PDA-PF**s) were synthesized via the radical polymerization of 4-diphenylaminostyrene (**1**) or monomer **1** and pentafluorostyrene (Scheme 1). Monomer **1** was synthesized via a palladium-catalyzed one-pot amination reaction of 4-aminostyrene and 4-bro-

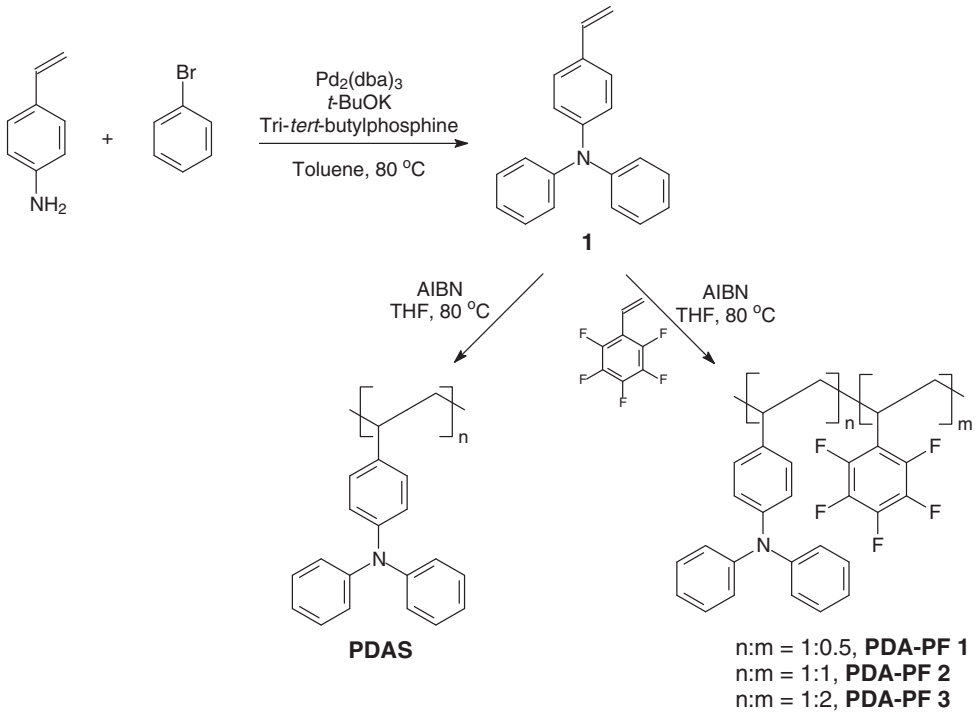

Scheme 1. Synthesis of 4-diphenylaminostyrene and triarylamine-based polymers.

Table 1
Properties of the triarylamine-based polymers.

Polymer	Yield (%)	Comonomer ratio (PDA:PF)		M_n (M_w/M_n)[b]	Fluorine content (%)[c]
		Feed	Found[a]		
PDAS	66	1:0	1:0	6 000 (2.3)	0
PDA-PF 1	55	1:0.5	1:0.6	17 000 (2.0)	5.7
PDA-PF 2	44	1:1	1:1.1	17 000 (1.8)	8.9
PDA-PF 3	53	1:2	1:1.8	20 000 (2.0)	12.1

[a] Calculated from the ^{1}H NMR spectra, by comparison of aromatic proton peaks at 6.30–7.32 ppm to vinyl proton peaks at 1.57–2.95 ppm.
[b] Measured by GPC vs. polystyrene standards.
[c] Percentage of the number of C–F bonds per the total number of bonds in the repeating unit.

mobenzene as reported in the literature [16]. To investigate the polarity changes of triarylamine-based polymers induced by variation of the fluorine content in the polymer structure, copolymers with various ratios of 4-diphenylaminostyrene (PDA) to pentafluorostyrene (PF) unit (1:2, 1:1 and 2:1) were prepared by controlling the feed ratio of each monomer. These feed ratios corresponded to values calculated by comparing the ^{1}H NMR peak integration ratio of the aromatic protons of the 4-diphenylaminostyrene unit and vinyl protons of the pentafluorostyrene unit (Table 1). To estimate the average molecular weight and polydispersity values, gel permeation chromatography was used. The molecular weight of **PDAS** is lower than those of **PDA-PF**s probably because the bulky triarylamine moieties near the vinyl groups, which sterically hinders the monomers from approaching the radical propagating species during radical polymerization, can limit the increase of the molecular weight of the homopolymers. In a comparative experiment, poly(penta-fluorostyrene) (**PFS**) (M_n = 7 700, M_w/M_n = 2.2 by GPC) was blended with TIPS pentacene and inkjet printed to investigate the influence of a highly fluorinated polymer structure on the phase separation behavior and its electrical performance of the TIPS pentacene-based OTFTs.

The inkjet-printing behavior of polymer/TIPS pentacene was studied by the investigation of the inkjet-printed polymer/TIPS pentacene single droplets and films by 3D profiling and α-step analysis. It is believed that the morphological behavior of the inkjet-printed single droplets consequently has an influence on the morphology of the final inkjet-printed films because the inkjet-printed polymer/TIPS pentacene films are composed of a lot of piled droplets. This means that the continuous inkjet-printing of single droplets can build up a number of printing lines, which can eventually develop the inkjet-printed films. As shown in Fig. 1, the "coffee-ring" effect of a convective flow was observed for all dried single droplets, which can control the final morphology of the inkjet-printed films. However, no remarkable variations in the height of each droplet edge in relation to the various polymers were observed. This is probably due

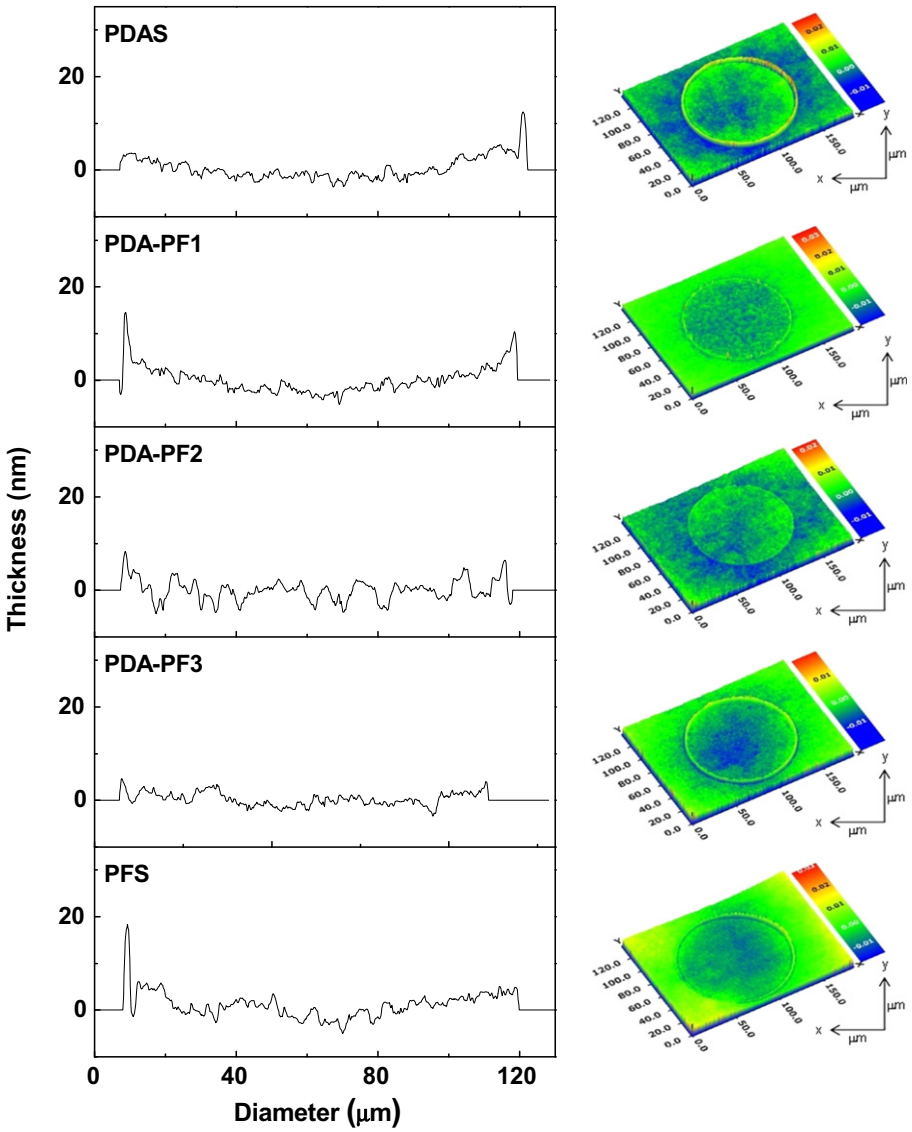

Fig. 1. The 3D profiler images of the inkjet-printed polymer/TIPS pentacene droplets.

Table 2
Characteristics of the inkjet-printed (at 25 °C) polymer/TIPS pentacene droplets and films.

Polymer	Droplet size (μm)[a]	Number of droplets/mm	Average film thickness (nm)[b]	R_a (nm)[b]
PDAS	119	78	530	126
PDA-PF 1	113	78	570	133
PDA-PF 2	111	78	500	140
PDA-PF 3	113	78	350	87
PFS	118	78	340	132

[a] Measured by a 3D surface profiler.
[b] Films were formed by a deposition of droplets by the inkjet-printing process and the thickness was measured by α-step by scanning five random lines in the area of 1000 μm^2.

to the fact that the surface tension gradient between the edge of the single drop and the center developed in each droplet should be identical for all polymer/TIPS pentacene droplets, because the boiling point and viscosity of the solution should be same or quite similar. This result indicates that the surface morphology of the inkjet-printed films in

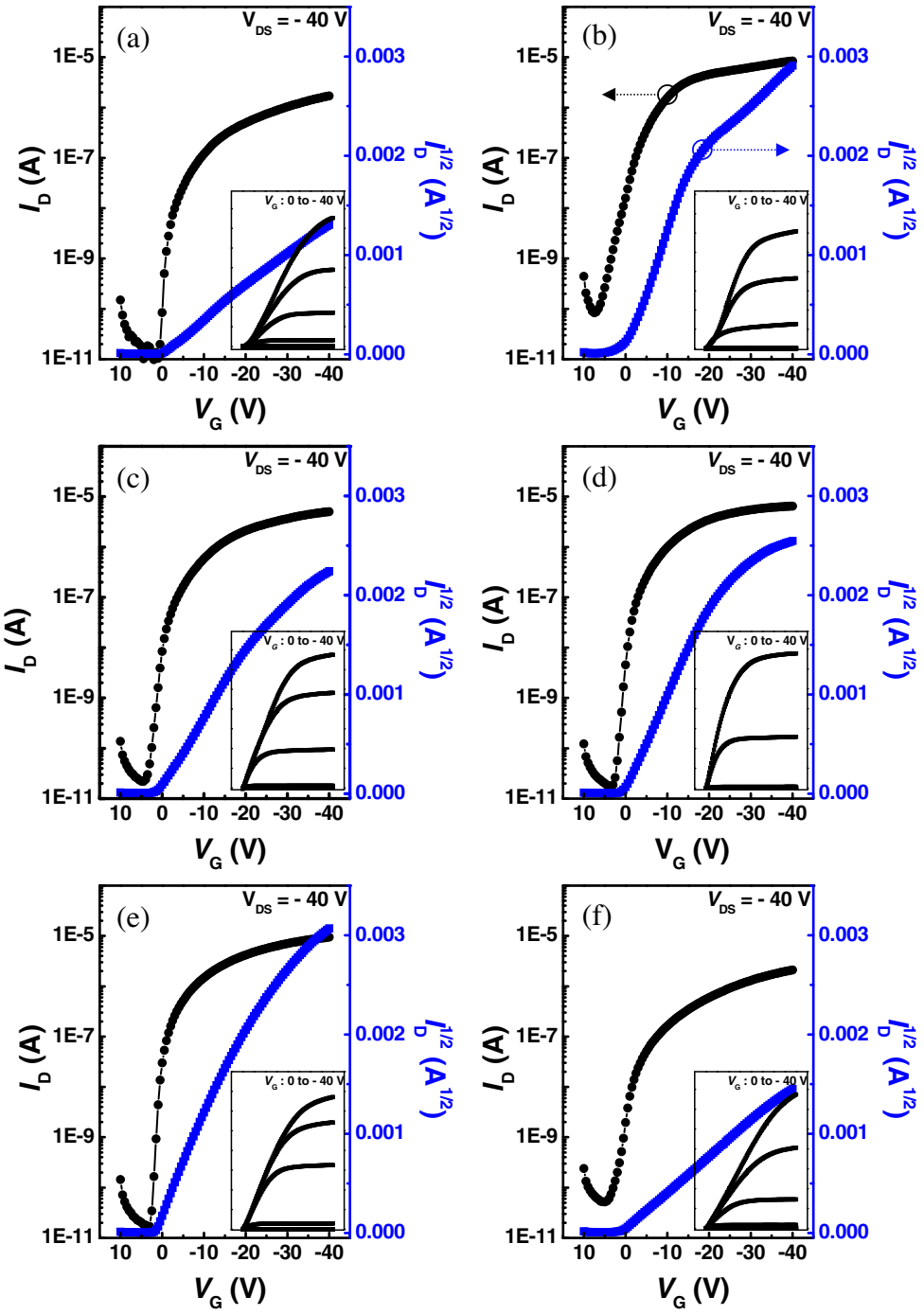

Fig. 2. The transfer and output characteristics of the polymer/TIPS pentacene TFTs fabricated using different polymers in an inkjet printing process: (a) pure TIPS pentacene, (b) **PDAS**/TIPS pentacene, (c) **PDA-PF 1**/TIPS pentacene, (d) **PDA-PF 2**/TIPS pentacene, (e) **PDA-PF 3**/TIPS pentacene, and (f) **PFS**/TIPS pentacene.

our experiment is more significantly affected by the TIPS pentacene crystal aggregates in the bulk films than the morphology of the single inkjet-printed droplets.

Measured single droplet sizes were approximately 110 μm and there were no significant differences in droplet size in relation to the polymer structure. It is quite natural that the inkjet-printing solutions that have similar boiling point and viscosity should create constant droplet sizes. The thickness of the final inkjet-printed films composed of piled droplets was in the range from 340 to 570 nm with high R_a values. As expected, non-uniform film properties are somewhat inevitable for the inkjet printing process [17]. In particular, it is expected that the phase separated TIPS pentacene crystal domains from the

Table 3
Characteristics of the polymer/TIPS pentacene TFTs.

Polymer	Polymer/TIPS pentacene ratio (w/w)[a]	Average mobility ($cm^2 V^{-1} s^{-1}$)[b]	Threshold voltage (V)	On/off ratio	Max. mobility ($cm^2 V^{-1} s^{-1}$)
–	0:1	0.069 ± 0.058	1.9 ± 2.9	6.2×10^4	0.15
PDAS	1:1	0.190 ± 0.027	−0.1 ± 0.8	9.0×10^5	0.23
PDA-PF 1	1:1	0.064 ± 0.013	−1.2 ± 1.4	2.5×10^5	0.084
PDA-PF 2	1:1	0.098 ± 0.039	−2.5 ± 1.8	4.5×10^5	0.15
PDA-PF 3	1:1	0.140 ± 0.018	1.0 ± 1.6	4.6×10^5	0.17
PFS	1:1	0.038 ± 0.009	−7.0 ± 2.1	4.4×10^4	0.046

[a] All samples were dissolved in toluene and inkjet printed.
[b] For 20 OTFT devices.

Table 4
Polar factor, solubility parameter, and Flory–Huggins parameter of triarylamine-based polymers.

Polymer	σ_p ($dyn\ cm^{-1}$)[a]	δ_2 ($(J\ cm^{-3})^{1/2}$)	χ_{12}[b]
PDAS	1.83	21.92	1.46
PDA-PF 1	1.60	19.63	0.01
PDA-PF 2	1.72	18.49	0.19
PDA-PF 3	3.38	17.34	0.98
PFS	19.08	15.05	4.35

[a] Measured from contact angles of water and diiodomethane on spin-coated polymer films.
[b] Calculated from $\delta_1 = 19.4\ (Jcm^{-3})^{1/2}$.

polymer domains can have a significant influence on this film uniformity in addition to the inkjet-printing process itself. The characteristics of the inkjet-printed single droplets and films are summarized in Table 2.

In the TFTs, a patterned ITO substrate was used as the gate electrode. This was covered by a film of cross-linked sulfur-based polymers by photo-curing, which acted as a gate insulator. The polymer/TIPS pentacene solution was then inkjet printed onto the gate insulator, and gold was subsequently deposited on the active layers for the source-drain electrodes. Fig. 2 shows the transfer and output characteristics of OTFTs that were prepared from the various polymer/TIPS pentacene blends. Table 3 summarizes the electrical characteristics of the TIPS pentacene-based OTFTs. In all the OTFTs, the output curves clearly exhibit a pinch-off and good current saturation (see inset of Fig. 2). Furthermore, as shown in Fig. 2 and Table 3, the electrical performance of the TIPS pentacene TFTs appears to depend quite strongly on the different structures of the blended polymers and the subsequent polarity variation. Interestingly, the average field-effect mobility of the **PDA-PF** blended TFT increases from 0.064 ± 0.013 to 0.14 ± 0.018 $cm^2 V^{-1} s^{-1}$ as the polymer structure possesses more C–F bonds (Table 1 and Table 3). On the other hand, the **PDAS** TFT was found to exhibit a slightly higher mobility than the **PDA-PF** TFTs, although the polar component of the surface energy of **PDAS** is similar or lower than those of **PDA-PF**s (Table 4).

To explain these results, we applied the Flory–Huggins theory to the polymer-blend organic semiconductor system. The Flory–Huggins interaction parameter, χ, is the energy change when one component (A) is removed from an area of pure A and is replaced with another component (B) from an area of pure B. Positive values of χ indicate that mixing A and B results in an increase in energy; therefore this mixing process is energetically unfavorable from an enthalpic standpoint. Negative values of χ indicate that mixing is energetically favorable. This means that χ is the measure of the segregation strength or miscibility between two components in the blended system. Traditionally, the Flory–Huggins interaction parameter can be estimated from the Hildebrand solubility parameters of the solvent (δ_1) and polymer (δ_2) and the solvent molar volume (V_1):

$$\chi_{12} = \frac{V_1(\delta_1 - \delta_2)^2}{RT} \tag{2}$$

Mutually soluble polymer/solvent pairs possess similar solubility parameters. As the difference between the solubility parameters increases, the tendency toward dissolution decreases [18].

The solubility parameters can be estimated by using additive group contribution theory. The definition of the solubility parameter is given in Eq. 3 in terms of the cohesive energy (E_{coh}), molar volume (V), and molar attraction constant (F). This equation yields a solubility parameter (δ):

$$\delta = \left(\frac{E_{coh}}{V}\right)^{1/2} = \frac{F}{V} \tag{3}$$

The cohesive energy represents the increase in internal energy per mole if all intermolecular forces are eliminated. Cohesive energies can be calculated from heats of vaporization for low molecular weight substances or from vapor pressure–temperature relationships. Due to difficulties in evaporating polymer materials, methods to predict the cohesive energy have been developed. Small, Van Krevelen, and Hoy developed group contribution values for the molar attraction constant F, which has additive qualities for low and high molecular weight materials. Hilderbrand solubility parameters for triarylamine based polymers were determined from the method of Van Krevelen. The Flory–Huggins parameters between TIPS pentacene and polymers were calculated from Eq. 2 based on the previously reported solubility parameter value (δ_1) of TIPS pentacene [19]. The polar components (σ_p) of the surface energy, solubility parameters (δ_2) for the polymers, and the Flory–Huggins parameters (χ_{12}) are summarized in Table 4.

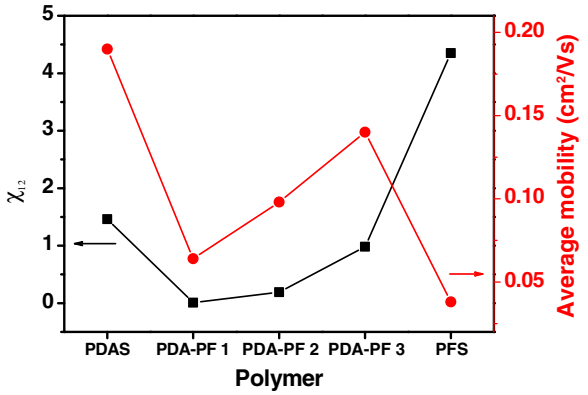

Fig. 3. Relationships between the average mobility of the polymer/TIPS pentacene TFTs and the Flory–Huggins interaction parameter.

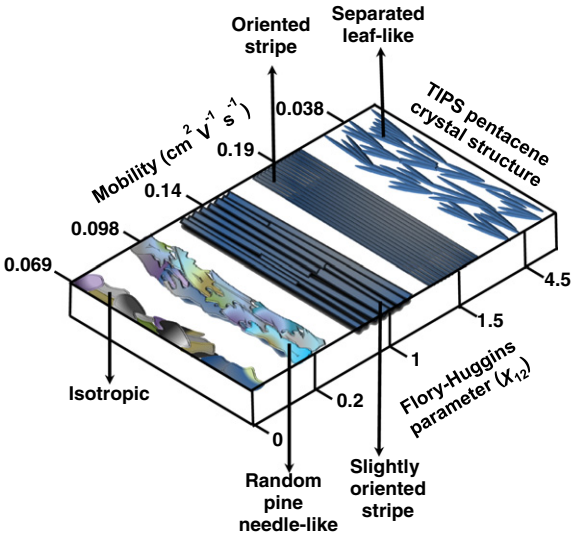

Scheme 2. Schematic diagram of various TIPS pentacene crystal structures with respect to the Flory–Huggins parameters and the measured mobility values.

Lodge and Hillmyer reported that the increase in the segregation strength (χ_{12}) is attributed to the increase in the polarity difference between the two blocks in poly(styrene-*b*-isoprene) diblock copolymers as the presence of C–F bonds introduces polarity in the fluorinated segments [20,21]. Given Lodge and Hillmyer's finding, our results showed that the increasing fluorine content in the polymer structure from **PDA-PF 1** to **PDA-PF 3** induced a larger χ value, which can bring about greater segregation between the polymer and TIPS pentacene. However, it was observed from the σ_p value of **PDAS** that the homopolymers with solely triarylamine pendant groups, which contains highly polar amine moieties, already retain enough polar nature. Therefore, the introduction of a relatively small number of fluorine groups cannot help increase the polarity in the polymer structure. Admittedly, the TFT characteristics of the polymer/TIPS pentacene TFTs are closely related to χ_{12} values, that is, the segregation strength between the polymer and the TIPS pentacene phase (Fig. 3). We believed that suitable or moderate segregation ($\chi_{12} \sim 1$) of the polymer region in the system could induce the highly oriented crystalline structure of TIPS pentacene. However, excessive strong segregation strength, as seen in **PFS** ($\chi_{12} \sim 4$), may disturb the orientation of crystals and further disconnect the channel pathways by means of the formation of tiny TIPS pentacene crystal structure.

To further understand the relationship between the measured OTFT properties and the phase separation behavior between the polymers and TIPS pentacene, polarized optical microscopy, 3D surface profile, and XRD were used to observe the crystal orientation, surface morphology, and crystallinity of the polymer/TIPS pentacene thin films. As shown in Fig. 4, the color of polarized light microscopy images varied depending on both crystal orientation and thickness. The crystals of inkjet-printed pure TIPS pentacene are highly anisotropic with various crystal

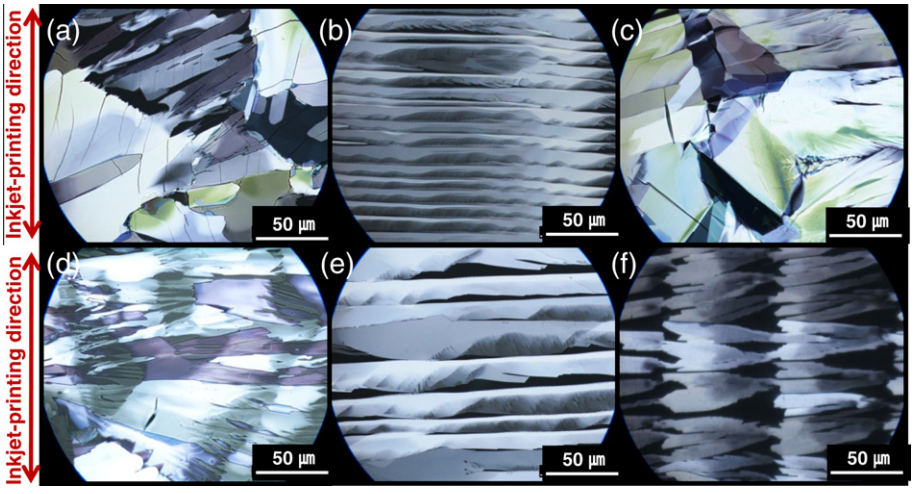

Fig. 4. Polarized optical microscopy images of inkjet-printed pure TIPS penatacene and the polymer/TIPS pentacene thin films: (a) pure TIPS pentacene, (b) **PDAS**/TIPS pentacene, (c) **PDA-PF 1**/TIPS pentacene, (d) **PDA-PF 2**/TIPS pentacene, (e) **PDA-PF 3**/TIPS pentacene, and (f) **PFS**/TIPS pentacene.

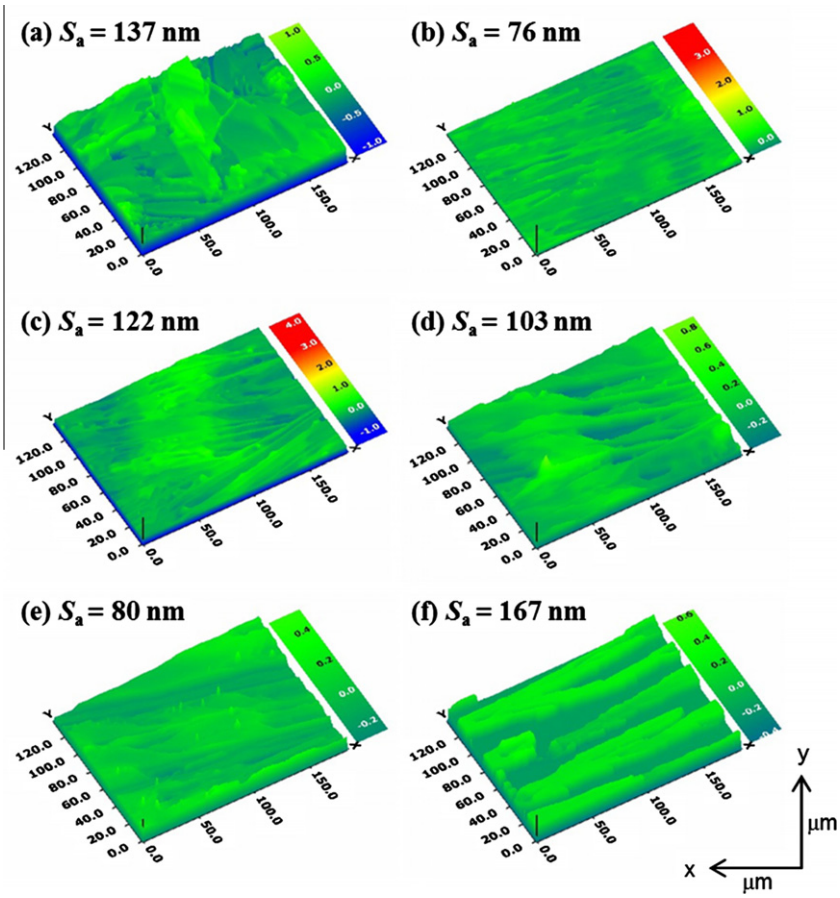

Fig. 5. Surface roughness of inkjet-printed pure TIPS penatacene and polymer/TIPS pentacene thin films: (a) pure TIPS pentacene, (b) **PDAS**/TIPS pentacene, (c) **PDA-PF 1**/TIPS pentacene, (d) **PDA-PF 2**/TIPS pentacene, (e) **PDA-PF 3**/TIPS pentacene, and (f) **PFS**/TIPS pentacene.

grain sizes, which is responsible for the wide range of measured mobility values from 0.026 to 0.15 $cm^2 V^{-1} s^{-1}$. When TIPS pentacene was blended with **PDAS** or **PDA-PF 3**, long needle or stripe-shaped crystal domains were observed with high crystalline orientation across the Au channel, while TIPS pentacene with **PDA-PF 1** or **PDA- PF 2** showed pine-needle-shaped crystal structure with random crystalline orientation. As a tendency for TIPS pentacene to segregate from the polymer phase is developed, stratification with highly oriented crystalline structure becomes dominant. In other words, TIPS pentacene crystals and amorphous polymer chains can be assembled separately within the layered structure if they cannot dissolve each other efficiently. We believe this stratification is a consequence of TIPS pentacene crystallization from the blend of the polymer/TIPS pentacene with the polymer segregation being driven by enthalpic interactions which is closely related to the Flory–Huggins interaction. When the segregation strength is quite strong, as in **PFS**/TIPS pentacene, the shape of the TIPS pentacene crystals was observed to be individual leaf-like. Although the crystals are well oriented, the large area of crystal grains cannot be connected continuously as seen in Fig. 4f, which can hamper charge transport between the channels. This means that excessive stratification caused by the excessive strong phase separation can induce the formation of a crystal archipelago composed of chopped crystal grains. Consequently, the electrical performance of the polymer/TIPS pentacene blends is highly dependent upon the crystalline morphology within the film, which is determined by the manner of phase separation. A schematic diagram of the TIPS pentacene crystal structures in relation to the Flory–Huggins parameters and measured mobility values is shown in Scheme 2.

It should be emphasized here that the inkjet-printed polymer/TIPS pentacene films are composed of numerous single printed droplets and that the inkjet-printing directions are orthogonal to the orientations of TIPS pentacene crystals for **PDAS** and **PDA-PF 3**. In addition, a continuous deposition of ink for the second printing line, which can partially overlap the first inkjet-printed line, should be carried out prior to the complete drying of the first inkjet-printed line, which process can induce the facile phase separation of TIPS pentacene crystals within the printed deposits. It can also be inferred that a crystal orientation perpendicular to the printing direction possibly originates from the upward or downward phase separation of the TIPS pentacene crystals in the highly overlapped areas of droplets in the vertically printed line. During the printing of the second line neighboring the first printed line, the

separated crystals in the original line can be connected horizontally to the crystal regions in the second printed line because the vertical position of all droplets is the same for all the printed lines. Therefore, we believe that such horizontal connections or mergers of crystal domains between neighboring printed lines can allow the evolution of an orthogonal orientation of the TIPS pentacene crystals to the printing direction. Considering the localized anisotropic character of the TIPS pentacene crystals in the case of the pure TIPS pentacene or of the **PDA-PF1**/TIPS pentacene with the same inkjet-printing directions and conditions, however, it should be concluded that the different phase separation behavior depending on the polymer structure is quite critical for the orientation of the TIPS pentacene crystals.

The surface morphology of the inkjet-printed polymer/TIPS pentacene films was observed by a 3D surface profiler as shown in Fig. 5. The polymers with higher χ_{12} values generally showed smoother surfaces, indicating lower S_a (the arithmetic average of the 3D roughness) value. The 3D surface profile images clearly show that, in comparison with the **PDA-PF 1** or **PDA-PF 2**/TIPS pentacene thin films, **PDAS** and **PDA-PF 3**/TIPS pentacene thin films possess much denser and smoother surfaces and have no discernible and non-oriented large crystal grain boundaries. This result indicates that irregular and anisotropic crystal domains which result from insufficient phase separation can have a significant influence on the surface morphology of inkjet-printed films. Note that the uneven surface roughness induced by the randomly distributed crystal plates of TFT film used as an active channel scatters electrons and reduces the mean free path of free electrons. Therefore, the coarse surface acts as a barrier to free electrons that move from the source to drain electrodes, which can lead to significant variations in device performance. A quite anisotropic and rough film surface appeared in the pure TIPS pentacene printed films and the strong segregation of TIPS pentacene from **PFS** domains generated an oriented but quite rough surface morphology. This rough surface and the sparsely disconnected channels produced by the isolated TIPS pentacene crystals can adversely affect TFT performance.

The XRD patterns in Fig. 6, which were obtained by a thin film diffraction method, show that the variation in the crystallinity of the polymer/TIPS pentacene films depends on the polymers used. The patterns consistently exhibit a strong (001) peak indicating typical TIPS pentacene crystal phase. Even though the film thickness of **PDA-PF 3** or **PFS**/TIPS pentacene is quite thin compared to that of other polymer/TIPS pentacene films (Table 2), the (001) peak showed a stronger intensity. In the case of the **PDA-PF 1** film with the thicker thickness, a weaker (001) peak was observed. Based on these results, the inclination of the peak intensities of the TIPS pentacene crystals, depending on different polymer structures in the blending system, can be analyzed reasonably without considering the influence of the film thickness on the XRD intensity. Unfortunately, we could not obtain any information about the horizontal crystal orientation of TIPS pentacene such as (100) peak for each polymer/TIPS pentacene film. However, it is noted that the degree of crystallinity of the film

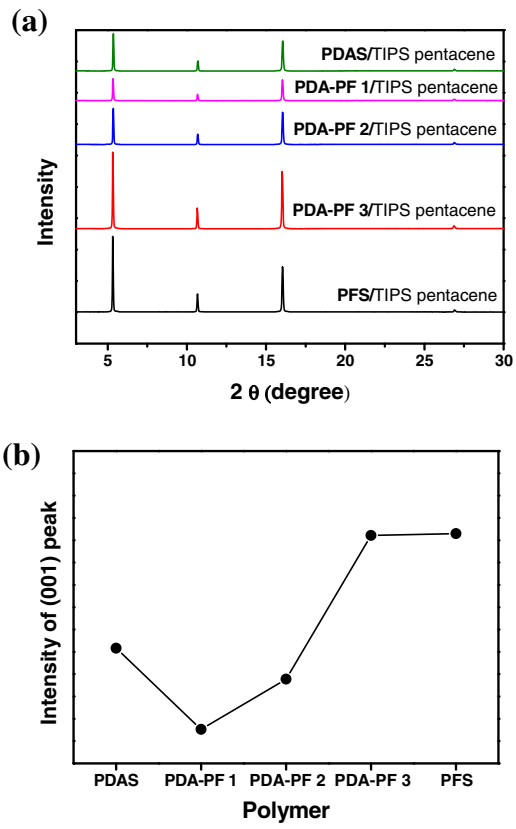

Fig. 6. (a) XRD patterns and (b) intensity of (001) peak of inkjet-printed polymer/TIPS pentacene.

generally increases as the segregation strength between the polymer and TIPS pentacene increases, as indicated by the increased intensity of (001) reflections (Fig. 6b). This result indirectly means that the formation of the microcrystalline structure of TIPS pentacene during the bulk phase segregation of TIPS pentacene from the polymer region can be affected by the degree of phase separation of each polymer. This may be due to the stronger crystal packing force or the highly oriented crystal structure caused by the stronger segregation strength. With the information from both optical microscopy and XRD, we conclude that high crystallinity and crystal orientation of TIPS pentacene can be achieved in moderately phase separated polymer/TIPS pentacene films.

4. Conclusions

We investigated how phase separation behavior between polymers and TIPS pentacene in polymer/TIPS pentacene blends influences the properties of TIPS pentacene-based TFTs. To examine various types of segregation, triarylamine-based polymers with various polarity values were synthesized and inkjet printed to fabricate OTFTs. The observed TFT performance values are closely related to the segregation strength that is dependent on each polymer structure, which can be explained by the Flory–Huggins parameters. When the polymer structure can induce

moderate phase separation between two phases, the OTFT showed considerably improved field-effect mobility of 0.14 to 0.19 $cm^2 V^{-1} s^{-1}$. On the other hand, polymers having too strong tendency to phase-separate from TIPS pentacene crystal domains result in poor TFT characteristics. Polarized optical microscopy images reveal that the well-oriented and stripe-shaped TIPS pentacene crystal structure which is beneficial to the movement of charges can be built up by proper phase separation between the polymer region and TIPS pentacene crystal domains. Comparing to these phenomena, excessively weak phase separation forms randomly oriented crystal structures with large crystal domains, and excessively strong segregation induces disconnected and chopped tiny crystals. This crystallization behavior also affects the surface morphology of inkjet-printed polymer/TIPS pentacene films as represented by 3D surface profile images. X-ray diffraction results demonstrate that the level of TIPS pentacene crystallinity can also be related with the phase separation behavior. With our approach, it should be possible to formulate organic semiconductors with good TFT performance whose solid properties can be fine-tuned by predicting the phase separation behavior of polymer/TIPS pentacene blends. Furthermore, the high TFT performances of new blends of triarylamine-based polymer/TIPS pentacene and the easy preparation of TFTs by inkjet printing confirm the potential application of the proposed system in the field of flexible printed electronics.

Acknowledgment

This work was supported by Basic Science Research Program through the National Research Foundation of Korea (NRF) funded by the Ministry of Education, Science and Technology (Grant number: 2011-0004799).

References

[1] H. Sirringhaus, Adv. Mater. 17 (2005) 2411.
[2] G.H. Gelinck, H.E.A. Huitema, E. Van Veenendaal, E. Cantatore, L. Schrijnemakers, J. Van der Putten, T.C.T. Geuns, M. Beenhakkers, J.B. Giesbers, B.H. Huisman, E.J. Meijer, E.M. Benito, F.J. Touwslager, A.W. Marsman, B.J.E. Van Rens, D.M. De Leeuw, Nat. Mater. 3 (2004) 106.
[3] E.J. Meijer, D.M. De Leeuw, S. Setayesh, E. Van Veenendaal, B.H. Huisman, P.W.M. Blom, J.C. Hummelen, U. Scherf, T.M. Klapwijk, Nat. Mater. 2 (2003) 678.
[4] D.W. Li, L.J. Guo, Appl. Phys. Lett. 88 (2006) 3.
[5] D.W. Li, L.J. Guo, J. Phys. D Appl. Phys. 4 (2008) 7.
[6] J.E. Anthony, J.S. Brooks, D.L. Eaton, S.R. Parkin, J. Am. Chem. Soc. 123 (2001) 9482.
[7] X.R. Li, B.K.C. Kjellander, J.E. Anthony, C.W.M. Bastiaansen, D.J. Broer, G.H. Gelinck, Adv. Funct. Mater. 19 (2009) 3610.
[8] R.L. Headrick, S. Wo, F. Sansoz, J.E. Anthony, Appl. Phys. Lett. 92 (2008) 3.
[9] J.H. Chen, C.K. Tee, M. Shtein, D.C. Martin, J.E. Anthony, Org. Electron. 10 (2009) 696.
[10] T. Ohe, M. Kuribayashi, R. Yasuda, A. Tsuboi, K. Nomoto, K. Satori, M. Itabashi, Kasahara, J. Appl. Phys. Lett. 93 (2008) 053303.
[11] J. Kang, N. Shin, D.Y. Jang, V.M. Prabhu, D.Y. Yoon, J. Am. Chem. Soc. 130 (2008) 12273.
[12] J. Smith, R. Hamilton, I. McCulloch, M. Heeney, J.E. Anthony, D.D.C. Bradley, T.D. Anthopoulos, Synth. Met. 159 (2009) 2365.
[13] R. Hamilton, J. Smith, S. Ogier, M. Heeney, J.E. Anthony, I. McCulloch, J. Veres, D.D.C. Bradley, T.D. Anthopoulos, Adv. Mater. 21 (2009) 1166.
[14] W.L.F. Armego, D.D. Perrin, In Purification of Laboratory Chemicals, 4th ed., Butterworth–Heinemann, Oxford, 1996.
[15] D. Knipp, R.A. Street, A.R. Volkel, Appl. Phys. Lett. 82 (2003) 3907.
[16] M.V. Nandakumar, J.G. Verkade, Tetrahedron 61 (2005) 9775.
[17] H. Minemawari, T. Yamada, H. Matsui, J. Tsutsumi, S. Haas, R. Chiba, R. Kumai, T. Hasegawa, Nature 475 (2011) 364.
[18] D.W. Van Krevelen, K. Te Nijenhuis, Properties of Polymers, 4th ed., Elsevier, Oxford, 2009.
[19] J. Chen, D.C. Martin, J.E. Anthony, J. Mater. Res. 22 (2007) 1701.
[20] Y. Ren, T.P. Lodge, M.A. Hillmyer, Macromolecules 33 (2000) 866.
[21] M.A. Hillmyer, T.P. Lodge, J. Polym. Sci. Polym. Chem. Ed. 40 (2002) 1.